Alternatives to Friction Coefficient: Role of Frictional Instabilities on Fine Touch Perception

Maryanne Derkaloustian[a], Pushpita Bhattacharyya[b], Truc Ngo[c], Joshua G. A. Cashaback[c], Jared Medina[b,d], Charles B. Dhong[a,c*]

[a]*Department of Materials Science and Engineering, University of Delaware, Newark, DE, USA*
[b]*Department of Psychological and Brain Sciences, University of Delaware, Newark, DE, USA*
[c]*Department of Biomedical Engineering, University of Delaware, Newark, DE, USA*
[d]*Department of Psychology, Emory University, Atlanta, GA, USA*

*Author to whom correspondence should be addressed: cdhong@udel.edu

Abstract

Fine touch perception is often correlated to material properties and friction coefficients, but the inherent variability of human motion has led to low correlations and contradictory findings. Instead, we hypothesized that humans use frictional instabilities to discriminate between objects. We constructed a set of coated surfaces with minimal physical differences that by themselves, are not perceptible to people, but instead, due to modification in surface chemistry, the surfaces created different types of instabilities based on how quickly a finger is slid and how hard a human finger is pressed during sliding. We found that participant accuracy in tactile discrimination most strongly correlated with formations of steady sliding, and response times negatively correlated with stiction spikes. Conversely, traditional metrics like surface roughness or average friction coefficient did not predict tactile discriminability. In fact, the typical method of averaging friction coefficients led to a spurious correlation which erroneously suggests that distinct objects should feel identical and identical objects should feel distinct. Identifying the central role of frictional instabilities as an alternative to using friction coefficients should accelerate the design of tactile interfaces for psychophysics and haptics.

Introduction and Background

People can readily distinguish and describe a variety of textures by touch, but there is no single material parameter or property that consistently predicts human fine touch. Fine touch arises from the friction generated between a finger and an object, so the most common method to classify objects in fine touch is by assigning a constant friction coefficient to different materials.[1,2] Although the friction coefficient is often convenient, it is not a material property[3] and most findings have yielded either contradictory results or low statistical correlations to human performance, like discriminability or identification.[4,5] The cause of these discrepant findings is, in part, that sliding friction in soft systems have significant oscillations in forces arising from microscale stick-slip, adhesion, and elasticity.[6] Indeed, the inherent human variability in finger velocity and pressure means that the variations in friction encountered on a single object can be larger than the variations in friction between two distinct objects.[7–9] Thus, the question we set to answer here is: how can humans rapidly distinguish objects despite inherent human variability in finger motion and resulting friction?

Instead of a material property or parameter, we hypothesized that humans could tell surfaces apart due to the likelihood of encountering frictional instabilities like stiction spikes and slow

friction waves. These frictional instabilities arise due to the competition between the elasticity of the finger and adhesion to a substrate.[6] In an experimental parameter space of finger pressure and velocity, the boundary where one instability type forms versus another is dependent upon surface composition.[8,10] We surmise that humans actively explore surfaces to find these transitions between different types of frictional instabilities to tell surfaces apart. Classifying surfaces based on transitions between instabilities would be advantageous because it is less variable than raw friction forces typically seen in macroscopic experiments.[10]

Most friction at solid interfaces is characterized by some degree of stick-slip behavior, where the fluctuations in force can largely depend upon sliding conditions as well as the material properties of each object.[11,12] In elastic, rigid systems, a critical spring constant dictated by sliding conditions and slip history can determine whether steady sliding or different forms of slip instabilities occur.[11,13] These rate and state laws gain even more complexity when one object is soft and deformable, and also makes adhesive contact with a hard surface. Prior to any slip events, the effects of contact aging are amplified with significant intermolecular forces at the interface,[14] and the drastic evolution of contact area while sliding largely controls the resulting friction force[15]. Additionally, local tensile and compressive stresses can often create periodic oscillations in this force, even in the absence of mesoscale interface detachment[16]. These phenomena are sufficiently explained for controlled systems with a constant normal load and known initial conditions, but the dynamics arising from the unconstrained nature of human touch and their mechanistic origins can be more difficult to predict.

Due to these systematic variations in friction, deriving relationships between a constant or average friction coefficient and tactile perception has led to low correlations or findings that do not generalize between studies. Typically, psychophysical studies using this approach rely on combining friction coefficients with other material properties and tactile dimensions defined by qualitative descriptors to extract correlations to participants' ability to distinguish between surfaces.[4,17] Instead, more direct correlations have often emerged from studies investigating dynamic friction during touch.[18,19] Gueorguiev *et. al*.[20] identify a partial slip region, where a finger's peripheral contact area begins to drop until a threshold of smoother sliding, as a strong tactile cue in discriminating between glass and PMMA slabs. However, the connections between their significant differences in physiochemical properties and their stick-slip behavior at the mesoscale remain unclear as these partial slips are dependent on finger velocity and pressure, and human fingers vary in both during free exploration.

Here, we investigate dynamic friction as a predictor across controlled surfaces to establish structure-dynamics-property relationships connecting molecular scale phenomena to mesoscale mechanics and elucidate fine touch perception. Within the ranges of applied finger pressures and sliding velocities observed in humans, the same material can exhibit multiple variations of stick-slip phenomena,[7,8,21] which challenges correlations derived from singular measurements of tangential force.

Mock finger as a characterization tool

In this work, we use a mechanical setup with a PDMS mock finger to derive tactile predictors from controlled friction traces alternative to average friction coefficients. While there is a tradeoff in selecting a synthetic finger over a more accurate, real human finger in modeling touch, our aim to design a method of mesoscale surface characterization for more successful studies on tactile perception cannot be fulfilled using one human participant as a standard. We believe that with

sufficient replication of surface and bulk properties as well as contact geometry, and controlled friction measurements collected at loading conditions observed during a tactile discrimination task, we can isolate unique frictional features of a set of surfaces that do not arise from human-to-human variability.

The major component of a human finger, by volume, is soft tissue (~56%),[22] resulting in an effective modulus close to 100 kPa.[23,24] In order to achieve this same softness, we crosslink PDMS in a 1×1×5 cm mold at a 30:1 elastomer:crosslinker ratio. However, two more features impart increased stiffness in a human finger. Most of this added rigidity is derived from the bone at the fingertip, the distal phalanx,[23–25] which we mimic with an acrylic bone within our PDMS network. The stratum corneum, the stiffer, glassier outer layer of skin,[26] is replicated with the surface of the mock finger glassified, or further crosslinked, after 8 hours of UV-Ozone treatment.[27] This treatment also modifies the surface properties of the native PDMS to align with those of a human finger more closely. It minimizes the viscoelastic tack at the surface, resulting in a comparable non-sticky surface. At least one day after treatment, the finger surface returns to moderate hydrophilicity (~60º), as is typically observed for a real finger.[28]

The initial contact area formed before a friction trace is collected is a rectangle of 1×1 cm. While this shape is not entirely representative of a human finger with curves and ridges, human fingers flatten out enough to reduce the effects of curvature with even very light pressures.[28–30] This implies that regardless of finger pressure, the contact area is largely load-independent, which is more accurately replicated with a rectangular mock finger. It is still a challenge to control pressure distribution with this planar interface, but non-uniform pressures are also expected during human exploration.

Lastly, we consider fingerprints vs. flat fingers. A key finding of our previous work is that while fingerprints enhanced frictional dynamics at certain conditions, key features were still maintained with a flat finger.[28] Furthermore, for some loading conditions, the more amplified signals could also result in more similar friction traces for different surfaces. We have continued to use flat fingers in our mechanical experiments, and have observed good agreement between these friction traces and human experiments.[7,8,21,31]

Materials and Methods

Surface Preparation

Silane coatings were prepared via chemical vapor deposition (CVD) onto 10 cm-diameter silicon wafers (University Wafer). Clean wafers were first treated with oxygen plasma (Glow Research Glow Plasma System) for 1 minute. They were immediately moved to a desiccator containing ~50 µL of silane (Gelest, 95-100% purity) on a glass slide. Alkylsilanes and aminosilanes each required a separate desiccator. After pulling vacuum, each desiccator was held under static vacuum for at least 4 hours. Evidence of plasma treatment as well as deposition was confirmed with atomic force microscopy (AFM), x-ray photoelectric spectroscopy (XPS), and water contact angle hysteresis experiments.

Atomic Force Microscopy

1×1 cm wafer pieces were imaged with a Bruker Multimode AFM to compare surface profiles of all silanes as well as the effects of plasma treatment. 10×10 µm scans were generated under tapping mode at a frequency of 1 Hz with tips of a ~120 kHz resonant frequency, and analyzed with Gwyddion microscopy data analysis and visualization software. All height profiles were processed

with a third-order background subtraction, a median height correction along the fast scanning (x) axis, and horizontal stroke correction prior to analysis. Aggregates were not masked as they only negligibly changed power spectral density profiles.

X-Ray Photoelectric Spectroscopy

To identify the elements present on our surfaces, 1×1 cm samples were scanned with a Thermo Scientific K-Alpha XPS system. 400 μm points were scanned on each sample, for individual elements C, N, O, and Cl, as well as an XPS survey scan.

Water Contact Angle Hysteresis

Advancing and receding angles of water droplets on our surfaces were measured using a goniometer (DSA14 Drop Shape Analysis System, Kruss). To measure advancing angles, ~3 μL of DI water was dispensed onto each surface, and an image of the droplet-surface interface was captured. ~1 μL of water was then slowly removed from the droplet such that it would recede, when another image was captured. Each droplet was fit to an automatic circle fit in ImageJ to obtain advancing and receding angles. This was repeated five times for each surface, in order to obtain average angles, and average hysteresis by subtracting the two.

Mock Finger Preparation

Friction forces across all six surfaces were measured using a custom apparatus with a polydimethylsiloxane (PDMS, Dow Sylgard 184) mock finger that mimics a human finger's mechanical properties and contact mechanics while exploring a surface relatively closely.[7,8] PDMS and crosslinker were combined in a 30:1 ratio to achieve a stiffness of 100 kPa comparable to a real finger, then degassed in a vacuum desiccator for 30 minutes. We are aware that the manufacturer recommended crosslinking ratio for Sylgard 184 is 10:1 due to potential uncrosslinked liquid residues,[32] but further crosslinking concentrated at the surface prevents this. The prepared PDMS was then poured into a 1×1×5 cm mold also containing an acrylic 3D-printed "bone" to attach applied masses on top of the "fingertip" area contacting a surface during friction testing. After crosslinking in the mold at 60ºC for 1 hour, the finger was treated with UV-Ozone for 8 hours out of the mold to minimize viscoelastic tack.

Mechanical Testing

A custom device using our PDMS mock finger was used to collect macroscopic friction force traces replicating human exploration.[7,8] After placing a sample surface on a stage, the finger was lowered at a slight angle such that an initial 1×1 cm rectangle of "fingertip" contact area could be established. We considered a broad range of applied masses (M = 0, 25, 75, and 100 g) added onto the deadweight of the finger (6 g) observed during a tactile discrimination task. The other side of the sensor was connected to a motorized stage (V-508 PIMag Precision Linear Stage, Physikinstrumente) to control both displacement (4 mm across all conditions) and sliding velocity (v = 5, 10, 25, and 45 mm s^{-1}). Forces were measured at all 16 combinations of mass and velocity via a 250 g Futek force sensor (k = 13.9 kN m^{-1}) threaded to the bone, and recorded at an average sampling rate of 550 Hz with a Keithley 7510 DMM digitized multimeter. Force traces were collected in sets of 4 slides, discarding the first due to contact aging. Because some mass-velocity combinations were near the boundaries of instability phase transitions, not all force traces at these given conditions exhibited similar profiles. Thus, three sets were collected on fresh spots for each condition to observe enough occurrences of multiple instabilities, at a total of nine traces per combination for each surface.

Instability Classification

Without any previously defined classifications of the instabilities in our systems, we restricted our force traces to 3 main types discussed in the main text: steady sliding, slow frictional waves, or stiction spikes. However, some stiction spikes were not immediately categorizable by eye, as performed independently by two coauthors, but consistency was maintained depending on whether these spikes were followed by steady sliding or slow frictional waves.

Pair Selection for Human Testing

With nine friction force traces for each mass-velocity pair and surface, large frequencies of instabilities could be counted and used to generate instability phase maps for each material. Frequencies of occurrence of steady sliding, stiction spikes, and slow frictional waves on each surface were determined manually, as well as total incidence of instabilities. These frequencies corresponded to color intensities for each instability on the phase maps, revealing similar zones but different boundaries for every surface.

The differences between these frequencies were calculated for several pairs, both previously tested and new pairs. Six pairs with a wide range of differences in total instabilities were selected, three of which had been tested prior to this work. These pairs had different ranges of individual instability differences as well, as shown in **Table 2**.

Human Testing

To verify that the differences in instabilities aid in tactile discrimination, we performed three-alternative forced choice tests (3-AFC) (N = 10 participants, n = 600 trials) on 10 sighted adult participants (IRB approval in **Acknowledgments**). In each trial, subjects were presented with three surfaces lined up horizontally to touch, two having the same silane coating and an odd sample out. Pairs as well as unique sample placement were randomized across all subjects and trials. No blindfolds or visual barriers were used since the appearances of all coatings were the same. Participants could touch for as long as they wanted, but were asked to only use their dominant index fingers along a single axis to better mimic the conditions for instability formation during mechanical testing with the mock finger. Once a participant made a final decision on which sample was unlike the other two, we input their answer in a premade Qualtrics form which recorded the time to the last click as the response time.

Results and Discussion

Generating Phase Maps of Frictional Instabilities

To test the hypothesis that humans use frictional instabilities to form tactile judgements, we constructed "minimal" tactile surfaces made from the vapor deposition of silanes onto silicon wafers for human testing (**Table 1**).

Table 1. Surface characterization of silanized silicon wafers.

Sample	Surface Structure	Average Roughness (R_a, pm)	Contact Angle (Advancing - Receding ± $\sigma_{Hysteresis}$, °)	Average Friction Coefficient ($\bar{\mu}$)	Friction Coefficient Interquartile Range (μ_{Q3} - μ_{Q1})	Hurst Exponent (H)

C4		861	(99.06-103.74) ± 2.5	2.21	1.24	0.56
C5	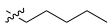	443	(100.18-109.68) ± 2.6	2.45	2.09	0.22
C6		858	(102.42-109.10) ± 5.1	2.49	1.74	0.29
C8	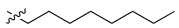	431	(108.38-114.32) ± 4.0	3.04	2.08	0.06
C4-APTMS	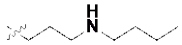	358	(54.74-59.44) ± 3.9	2.06	1.20	0.04
APTMS	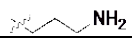	280	(49.80-58.28) ± 5.7	2.03	1.54	0.15

We describe these samples as "minimal" because the physical variations in roughness are below the human limits of detection[33,34] and the bulk and thermal properties of all samples are identical at the human scale because the silanes form a thin layer of order nanometers thickness.[35,36] Thus the only present differences in these samples are from those in surface chemistry (**Table 1**, see **SI** for details). We propose that the role of these differences in surface chemistry is to shift the boundaries between frictional instabilities to different finger pressures and velocities. As there is no existing method to accurately predict phase maps of instabilities of elastic bodies from molecular structure, we experimentally determined these frictional instability maps through a mechanical apparatus with a mock finger (**Fig. 1**).

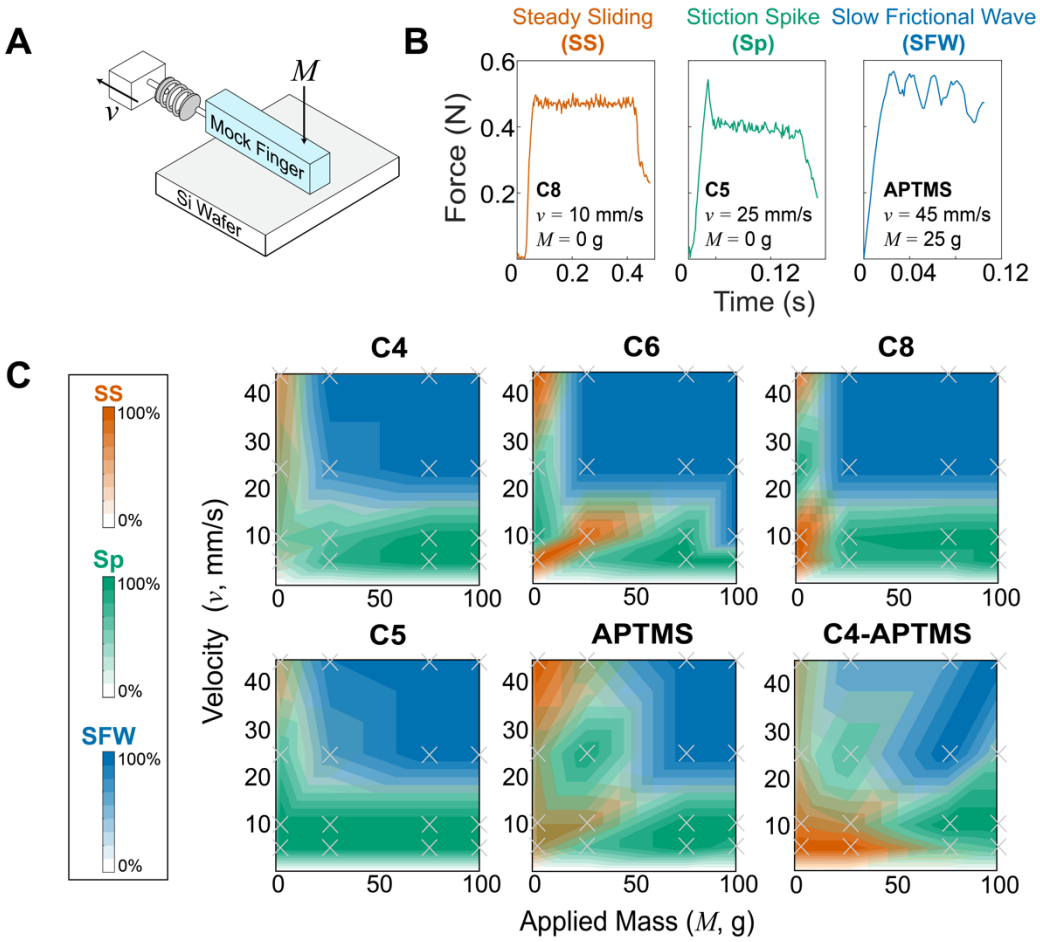

Fig. 1. Mechanical testing and determination of frictional instability landscape in samples. A) Schematic of friction testing apparatus. An elastomeric mock finger is connected to a force sensor and motorized stage. The mock finger was driven at four different driving velocities (v = 5-45 mm/s) at four different applied masses (M = 0-100 g, in addition to the deadweight of the mock finger), mimicking human exploration. B) Representative force curves of three types of frictional instabilities. *Steady sliding*, (**SS**, orange) shows no distinctive feature besides high frequency force oscillations due to stick-slip, which is above the electronic sensor noise. *Slow frictional waves* (**SFW,** blue) are slower, large amplitude oscillations corresponding to global or coherent stick-slip of the entire mock finger. *Stiction spike* (**Sp,** green) is where a single, large-magnitude stick-slip event is observed at the onset of steady sliding. C) Phase maps of frictional instabilities across all surfaces. Colors and intensities correspond to the type and frequency of each instability respectively at a given condition. Color map created by linear interpolation between experimental conditions, with location of conditions tested indicated by gray (×) marks.

Across the six different surface coatings and 16 different combinations of finger sliding velocity and applied mass, we observed that the friction traces could be categorized into three broad phases, which conceptually originate from the competition between the adhesion and elasticity of the finger. The first phase, *steady sliding* (**SS,** orange in **Fig. 1B**), shows a nearly constant friction force, except for high-frequency mechanical oscillations.[29,37] Mechanistically, this represents sufficient dissipation of kinetic energy relative to driving velocity, thus there is a lack of macroscale or concerted stick-events that lead to large oscillations in force.[20,29] Instead, microscale stick-slip events result in a high frequency, but small, oscillation around a comparatively steady mean. We observe that this occurs primarily at low applied masses, but different velocity zones depending on the surface. The initial slope in the steady sliding regime, and in all other phases is equal to k_{finger}. The second phase, *slow frictional waves* (**SFW,** blue in **Fig. 1B**), manifest as large oscillations in friction force with frequencies lower than any representative timescale for microscopic stick-slip or motor velocity. These oscillations are much larger than electronic noise of ~0.04 N. Slow frictional waves represent a scenario where kinetic energy by friction and adhesion is not dissipated sufficiently quick. Instead, stresses within the mock finger can localize to form instabilities like buckling,[38] pulses,[39] or wrinkling[40] to relieve the buildup of elastic stresses. We observe that slow frictional waves occurred more frequently at higher masses and velocities compared to steady sliding. This is expected because higher normal loads increase the tangential forces required for motion, and the higher velocities give shorter times to resolve stress irregularities.[41] We also observed a third phase, a singular *stiction spike* (**Sp,** green in **Fig. 1B**), that precedes an otherwise smooth, or if also exhibiting a slow frictional wave, comparatively small oscillating trace. This stiction spike represents where the initial barrier to motion, adhesion, represents a significant threshold above the mean sliding friction,[42] likely because most of these microscale contacts are broken within a short interval. Stiction spikes were routinely observed even after we discarded the first pull out of a sequential series of four pulls to remove the influence of contact aging originating from setup preparation. Stiction spikes are not necessarily mutually exclusive to steady sliding and slow frictional waves and can coexist with the others (see **Fig. S4** of **SI**). However, based on our heuristic classification scheme, a 10% higher spike than the mean during steady sliding was considered a stiction spike trace. When the spike was followed by slow frictional waves, the traces with the first peak being 40% higher in amplitude were also classified as stiction spikes.

In many cases, we observed that several trials in the same conditions consistently led to mixed phases, despite initially assuming that these originated from experimental error. Upon construction of the phase maps, we saw that mixed phases occur predominantly at boundaries. Conversely, in the interior, we see higher consistency (darker shade). Generally, we see that steady sliding is less frequent in short chained, unaligned surfaces like **C4** and **C5** (see Hurst exponents in **Table 1**). Although no analytical modeling of soft, mesoscale friction analysis has provided accurate phase maps of these instabilities, theoretical work[10] by Putelat *et. al.* and experimental work by others[16,43] have shown that these instability phase maps can have abrupt transitions.

As **Fig. 1** was constructed from friction measurements, we can also calculate an average friction coefficient, $\bar{\mu}$, by averaging the friction coefficient obtained at each of the 16 combinations of masses and velocities (**Table 1**). This calculation is a standard approach in tactile studies for summarizing friction measurements, or in some cases, surfaces are never characterized at multiple masses and velocities. However, summarizing friction data in this manner has been considered as conceptually questionable by others from a mechanics perspective.[3] **Fig. 1** shows that the type of instabilities and friction forces encountered on a single surface can vary widely depending on the conditions. As a result, large variations in the friction coefficient are expected, depending on the mass and velocity — even though measurements originate from the same surface. This variability in friction coefficient can be seen with the large interquartile range of friction coefficients, which shows that the variation in friction coefficient across a single surface is similar, or even larger, than the differences in average friction coefficient across two different surfaces. The observation that friction coefficients vary so widely on a single surface calls into question the approach of analyzing how humans may perceive two different objects based on their average friction coefficients.

Human participants testing.

The results from **Fig. 1** demonstrate that we can design human experiments with different pairs of surfaces with differential frequencies in the occurrence of instabilities. To determine if humans can detect these three different instabilities, we selected six pairs of surfaces to create a broad range of potential instabilities present across all three types. These are summarized in **Table 2**, where the first column for each instability is the difference in that instability formed between each pair, and the second is the percent difference. The percentages are determined by, in an example, **C4** has steady sliding in 23 out of 144 mechanical pulls and **C4-APTMS** has steady sliding occurring in 43 pulls. Thus, when comparing **C4** versus **C4-APTMS**, they have a difference in steady sliding of 20 out of a maximum 144 pulls, for a **|ΔSS|** of 13.9%. The absolute value is taken to compare total differences present, as the psychophysical task does not distinguish between sample order.

Table 2. Pairs of samples for human testing by their frequency of instability formation.

Label	Sample Comparison	|ΔSS|		|ΔSFW|		|ΔSp|	
		Count	%	Count	%	Count	%
P1	**C4** *vs* **C4-APTMS**	20	13.9%	16	11.1%	4	2.78%
P2	**C6** *vs* **C4-APTMS**	9	6.25%	27	18.8%	14	9.72%
P3	**C4** *vs* **C5**	11	7.64%	21	14.6%	14	9.72%
P4	**C8** *vs* **C4-APTMS**	14	9.72%	34	23.6%	2	1.39%
P5	**C4** *vs* **APTMS**	24	16.7%	16	11.1%	8	5.56%
P6	**C5** *vs* **C4-APTMS**	31	21.5%	23	16.0%	18	12.5%

10 participants were asked to perform a three alternative-forced choice task (3-AFC, n = 600 total trials), where they are given three samples at a time, two of which have the same surface coating, and one of which has a different coating — the identity and placement of the "odd-man out" sample was randomized. Participants were asked to select which of the one coating is unlike the other, which is advantageous because participants were not prompted to select based on potentially subjective percepts, such as which one feels "smoother" or "rougher".[44] To prevent any confounding effects from surface fouling by finger residue,[21,45] all samples were used only a single time. Blindfolds were unnecessary as all samples are visually identical. Additional testing details are provided in **Materials and Methods**.

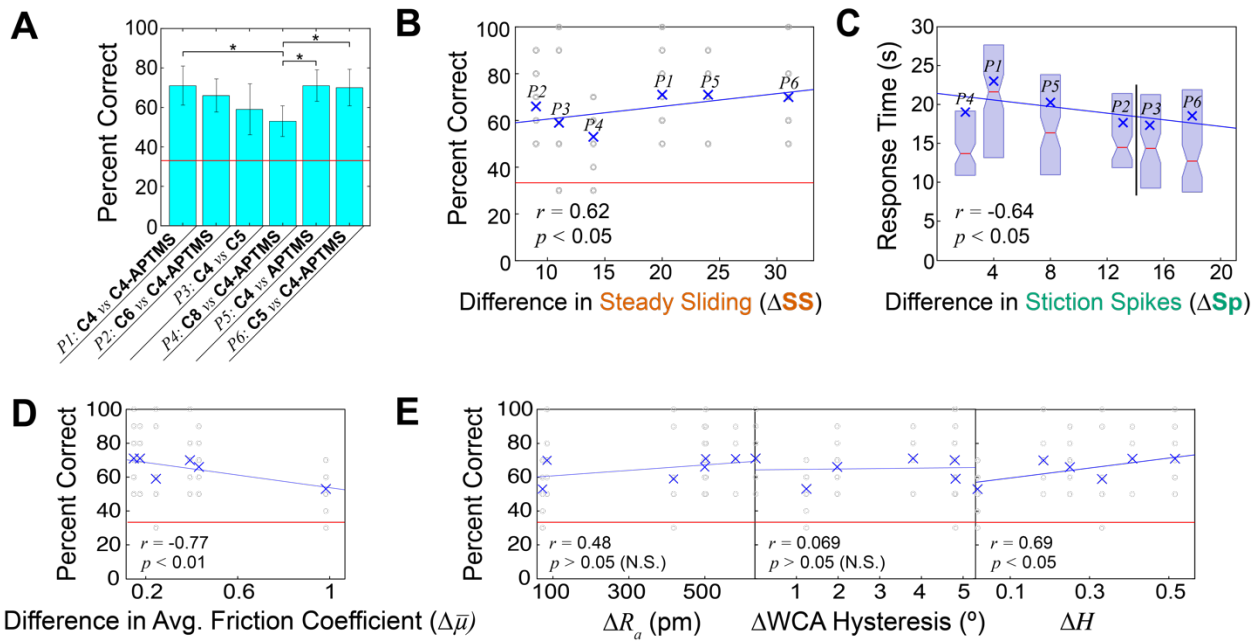

Fig. 2. Human subjects testing for discriminability between surfaces. A) Average accuracies of all pairs in a 3-AFC task. All pairs were statistically significantly distinguishable above chance (red line, 33%). Error bars are represented as 95% confidence intervals around the means. Ends of brackets with (*) above denote statistically significantly different accuracy rates. B) Generalized linear mixed model (GLMM) of accuracy vs. the differences in steady sliding events. Accuracies of each trial across all subjects represented by gray ○ marks, and global averages represented by blue × marks. C) GLMM of response times vs. the differences in stiction spike events. *P2* and *P3* have the same x-axis value and are shifted for clarity. Mean times are represented by blue (×) marks, while medians are represented by red lines at notches of box plots. D) GLMM of accuracy vs. difference in average friction coefficient ($\Delta\bar{\mu}$), showing a negative correlation. E) GLMMs of accuracy vs. other commonly used material properties or parameters: ΔAverage roughness R_a, ΔHurst exponent H, and ΔWater contact angle hysteresis (°) (N = 10 participants, n = 600 total trials).

Participants were successful in distinguishing between all pairs (**Fig. 2A**), with all average accuracies above chance (33%, $p < 0.005$ by one-sample t-test). There were statistically significant differences in performance across some pairs ($p < 0.05$, Wilcoxon rank sums) as indicated in **Fig.**

2A. Pairs which had similar accuracies are still insightful: as a conceptual example, participants had nearly the same accuracy with *P1* and *P6*, but from Table 2, *P1* had small differences (2.78%) in stiction spike production, whereas *P6* had large differences (12.50%).

We used the differential frequencies of each instability in Table 2 to perform a statistical fit of participant results by using a generalized linear mixed model (GLMM, details in **SI**). Considering all instabilities individually, we found that only steady sliding was a positive, statistically significant predictor. ($r = 0.62$, $p < 0.05$, shown in **Fig. 2B**). A positive correlation means that the more differences in steady sliding formation between a pair of material leads to higher accuracy in discrimination. Multi-term models including multiple instabilities were not statistically significant. Furthermore, a model accounting for slow frictional waves alone specifically shows a significant, negative effect on performance ($p < 0.01$, **Fig. S5 of SI**), suggesting that in these samples and task, the type of instability was not as important. Thus, forming either type of instability (slow frictional waves or stiction spikes) on one surface compared to another surface which consistently generates steady sliding will lead to two surfaces feeling very distinctive.

Average response times for each pair were also fit to a GLMM to determine if the type of instability affected decision-making speeds. Participants were quicker to discriminate between surfaces as differences in stiction spike production increased ($p < 0.05$, shown in **Fig. 2C**), while there was no significant relationship between steady sliding or slow frictional waves on response times. This may be because stiction spikes are the most prevalent instability in all surfaces except **C6**, so occurrences of steady sliding or slow frictional waves against a background of stiction spikes may be important in forming tactile judgements. Supporting the idea that deviances from stiction spike occurrence were important, we found that they were not a predictor of subject accuracy, only response time.

To compare the value of looking at frictional instabilities, we also performed GLMM fits on common approaches in the field, like a friction coefficient or material property typically used in tactile discrimination, shown in **Fig. 2D-E**. Interestingly, in **Fig. 2D**, we observed a spurious, negative correlation between friction coefficient (typically and often problematically simplified as $F = \bar{\mu}N$ across all tested conditions) and accuracy ($r = -0.64$, $p < 0.01$); that is, the more different the surfaces are by friction coefficient, the less people can tell them apart. This spurious correlation would be the opposite of intuition, and further calls into question the common practice of using friction coefficients in touch-related studies. The alternative, two-term model which includes adhesive contact area for friction coefficient[29] was even less predictive (see **Fig. S6A** of **SI**). We believe such a correlation could not have been uncovered previously as our samples are minimal in their physical variations. Yet, the dynamic changes in force even within a single sample are not considered, despite being a key feature of mesoscale friction during human touch.

We investigate different material properties in **Fig. 2E**. Differences in average roughness R_a (or other parameters, like root mean square roughness R_{rms} (**Fig. S6A** of **SI**) did not show a statistically significant correlation to accuracy. Though roughness is a popular parameter, correlating any roughness parameter to human performance here could be moot: the limit of detecting roughness differences has previously been defined as 13 nm on structured surfaces[33] and much higher for randomly rough surfaces,[46] all of which are magnitudes larger than the roughness differences between our surfaces. The differences in contact angle hysteresis – as an approximation of the adhesion contributions[47] – do not present any statistically significant effects on performance.

Interestingly, a large and statistically significant correlation is observed with the Hurst exponent H ($p < 0.05$), indicating differences in monolayer ordering are also likely to create distinct tactile feedback. This was expected since our silane-derived coatings cause frictional

differences due to monolayer ordering.[48,49] However, the Hurst exponent was positively correlated with response time (see **Fig. S6B** of **SI**), indicating that bigger differences in Hurst led to slower decision times which is counterintuitive. Thus, while Hurst exponent seems to work for accuracy in the surfaces here, it may not be generalizable to other types of surfaces.

Confirming Instability Formation During Human Exploration.

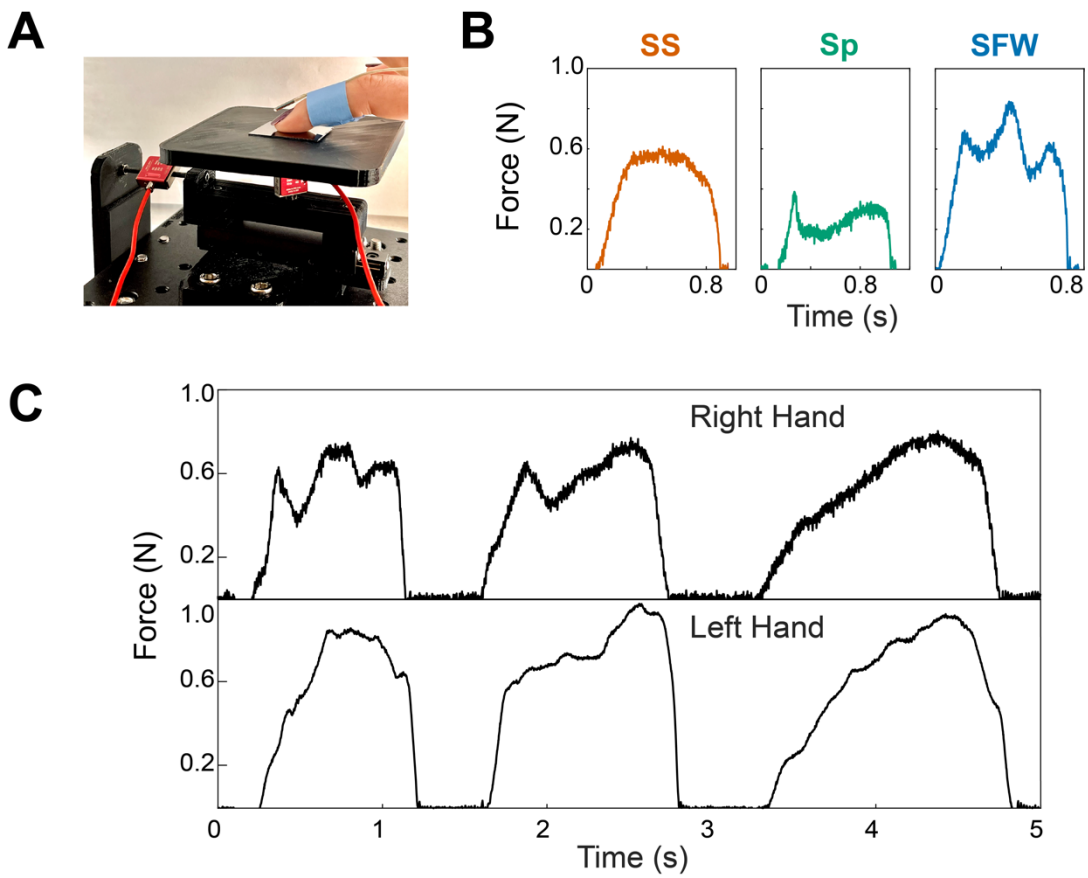

Fig. 3. Recording friction of a human finger exploring a surface. A) Setup to measure tangential and normal forces during fine touch. A coated sample is securely double-sided taped to a stage, connected to two red sensors to record tangential and normal forces. A motion tracker is also placed on the moving finger to record displacement while sliding. Two setups are used simultaneously, one for each hand. B) Formation of all instability phases during human exploration. C) Tangential forces experienced by two hands on the same surface chemistry.

To confirm that humans indeed form similar instabilities as the mock finger during exploration, we measured the tangential and normal force during a two-alternative forced choice (2-AFC) task. The participant placed their hands on a sensor stage, with one sample of **APTMS** under one hand and one sample of **C4** under the other. (**Fig. 3A**) The participant was then asked to explore each sample simultaneously, and ran over each surface in strokes along a single axis until the participant could decide which of the two had "more friction". **Fig. 3B-C** shows forces generated duration exploration. As expected, the participant had higher variability in their force trace than a mock finger. Yet despite this variability, we see that friction instabilities identified in the mock finger are also present in the human finger. We observe characteristic formation of steady sliding, slow

frictional waves, and stiction spikes. Slow frictional waves are notable because people are unlikely to intentionally oscillate their finger in such a rapid (~5 Hz) and consistent manner, especially since they were given no instruction to intentionally form the oscillations and generally slid their finger in a single motion.

Conclusions

Here, participants freely explored tactile minimal surfaces, which would not be expected to feel different to people based on nearly any common metric used in tactile perception. We further removed any confounding factors by asking participants to perform a low-level discrimination task, i.e., "which one does not feel like the others?", instead of a subjective percept, like "which one feels rougher?". We found that frictional instabilities explained how people are able to distinguish between the pairs found here. In these instabilities, we saw that stiction spikes drove how quickly participants decided between two surfaces. However, it was steady sliding that led to positive identification between surfaces, and slow frictional waves were negatively correlated and led to lower accuracy. This could be because slow frictional waves seemed to generally occur in the same exploration conditions. Thus, to create two surfaces that rapidly feel different, one limit could be a surface that only produces steady sliding versus stiction spikes. An example of this might be an oil- lubricated surface (steady sliding) versus a high-adhesion surface, like a freshly plasma-treated wafer.[50,51]

Instabilities are generated in a human finger, and the transitions between phases in different surfaces bridge the gap between the length scales relevant to molecular and mechanical phenomena. Instabilities may also help explain some aspects of tactile constancy, or the ability to retain object recognition properties despite varying environmental or human factors,[52,53] because instabilities themselves can be mathematically invariant to mass or velocity under certain conditions. In contrast, the raw friction force for a given experiment will vary with almost any input,[54] especially in macroscopic friction testing. Although the data gathered here came from a comparatively simple, single force sensor, we were still able to identify a trend that held across multiple substrates, which has been a longstanding challenge in the field. More sophisticated techniques, like spatially resolved force maps from digital image correlation[55] could benefit from categorizing instabilities' features. We note that despite collecting controlled mechanical force traces and then fitting to human performance, we still obtained high correlations, suggesting that we are capturing an important predictive phenomenon for future models of human touch. In comparison, other studies using direct measurements on humans have shown lower correlations,[4,18,20] and therefore could not isolate the most significant surface characteristics for discriminability, despite having obtained direct human measurements.

At this stage, it is not possible, *a priori*, to predict instabilities to a high degree of accuracy on real, experimental systems. Thus, characterizing surfaces by frictional instabilities will require mechanical testing. However, for those designing tactile interfaces in haptics or consumer goods, or extracting features in tactile arrays and soft robotics, analyzing existing force data along instabilities may be more predictive than traditional material properties and more consistent than raw friction traces.

Acknowledgments

We acknowledge support from the National Eye Institute of the NIH (R01EY032584-03). XPS was conducted at the Surface Analysis Facility at the University of Delaware (NSF CHE-

1428149). Atomic force microscopy was conducted at the Delaware Biotechnology Institute's Bio-Imaging Center at the University of Delaware supported by grants from the NIH-NIGMS (P20 GM103446), the NSF (IIA-1301765), and the State of Delaware. J.G.A.C. is supported by NSF CAREER award 2234748. This study was conducted and approved by the Institutional Review Board of the University of Delaware (Project #1484385-7), with data from 10 healthy participants between the ages of 21 and 32.

Competing Interest Statement

The authors declare no conflicts of interest.

References

1 A. M. Smith and S. H. Scott, *J. Neurophysiol.*, 1996, **75**, 1957–1962.
2 H. Khamis, H. M. N. Afzal, J. Sanchez, R. Vickery, M. Wiertlewski, S. J. Redmond and I. Birznieks, *J. Neurophysiol.*, 2021, **125**, 809–823.
3 O. Ben-David and J. Fineberg, *Phys. Rev. Lett.*, 2011, **106**, 254301.
4 L. Skedung, K. L. Harris, E. S. Collier and M. W. Rutland, *Exp. Brain Res.*, 2020, **238**, 1511–1524.
5 X. Zhou, J. L. Mo, Y. Y. Li, Z. Y. Xiang, D. Yang, M. A. Masen and Z. M. Jin, *Tribol. Lett.*, 2020, **68**, 85.
6 C. J. Rand and A. J. Crosby, *Appl. Phys. Lett.*, 2006, **89**, 261907.
7 A. Nolin, A. Licht, K. Pierson, C.-Y. Lo, L. V. Kayser and C. Dhong, *Soft Matter*, 2021, **17**, 5050–5060.
8 A. Nolin, K. Pierson, R. Hlibok, C.-Y. Lo, L. V. Kayser and C. Dhong, *Soft Matter*, 2022, **18**, 3928–3940.
9 Y. Peng, C. M. Serfass, A. Kawazoe, Y. Shao, K. Gutierrez, C. N. Hill, V. J. Santos, Y. Visell and L. C. Hsiao, *Nat. Mater.*, 2021, **20**, 1707–1711.
10 T. Putelat, J. H. P. Dawes and A. R. Champneys, *Proc. R. Soc. Math. Phys. Eng. Sci.*, 2017, **473**, 20160606.
11 J. R. Rice and A. L. Ruina, *J. Appl. Mech.*, 1983, **50**, 343–349.
12 T. Shoaib, J. Heintz, J. A. Lopez-Berganza, R. Muro-Barrios, S. A. Egner and R. M. Espinosa-Marzal, *Langmuir*, 2018, **34**, 756–765.
13 A. Ruina, *J. Geophys. Res. Solid Earth*, 1983, **88**, 10359–10370.
14 D. Petrova, D. K. Sharma, M. Vacha, D. Bonn, A. M. Brouwer and B. Weber, *ACS Appl. Mater. Interfaces*, 2020, **12**, 9890–9895.
15 R. Sahli, G. Pallares, C. Ducottet, I. E. Ben Ali, S. Al Akhrass, M. Guibert and J. Scheibert, *Proc. Natl. Acad. Sci.*, 2018, **115**, 471–476.
16 K. Viswanathan, N. K. Sundaram and S. Chandrasekar, *Soft Matter*, 2016, **12**, 5265–5275.
17 J. Dacleu Ndengue, I. Cesini, J. Faucheu, E. Chatelet, H. Zahouani, D. Delafosse and F. Massi, *IEEE Trans. Haptics*, 2017, **10**, 409–417.
18 L. Willemet, K. Kanzari, J. Monnoyer, I. Birznieks and M. Wiertlewski, *Proc. Natl. Acad. Sci.*, 2021, **118**, e2109109118.
19 C. Schwarz, *Trends Neurosci.*, 2016, **39**, 449–462.
20 D. Gueorguiev, S. Bochereau, A. Mouraux, V. Hayward and J.-L. Thonnard, *Sci. Rep.*, 2016, **6**, 25553.

21 Z. Swain, M. Derkaloustian, K. A. Hepler, A. Nolin, V. S. Damani, P. Bhattacharyya, T. Shrestha, J. Medina, L. Kayser and C. Dhong, *J. Mater. Chem. B*, DOI:10.1039/D4TB01646G.
22 M. Murai, H.-K. Lau, B. P. Pereira and R. W. H. Pho, *J. Hand Surg.*, 1997, **22**, 935–941.
23 A. Abdouni, M. Djaghloul, C. Thieulin, R. Vargiolu, C. Pailler-Mattei and H. Zahouani, *R. Soc. Open Sci.*, DOI:10.1098/rsos.170321.
24 P.-H. Cornuault, L. Carpentier, M.-A. Bueno, J.-M. Cote and G. Monteil, *J. R. Soc. Interface*, DOI:10.1098/rsif.2015.0495.
25 K. Qian, K. Traylor, S. W. Lee, B. Ellis, J. Weiss and D. Kamper, *J. Biomech.*, 2014, **47**, 3094–3099.
26 Y. Yuan and R. Verma, *Colloids Surf. B Biointerfaces*, 2006, **48**, 6–12.
27 Y.-J. Fu, H. Qui, K.-S. Liao, S. J. Lue, C.-C. Hu, K.-R. Lee and J.-Y. Lai, *Langmuir*, 2010, **26**, 4392–4399.
28 C. Dhong, L. V. Kayser, R. Arroyo, A. Shin, M. Finn, A. T. Kleinschmidt and D. J. Lipomi, *Soft Matter*, 2018, **14**, 7483–7491.
29 J. N. Israelachvili, *Intermolecular and Surface Forces*, Academic Press, 2011.
30 J. Gao, W. D. Luedtke, D. Gourdon, M. Ruths, J. N. Israelachvili and U. Landman, *J. Phys. Chem. B*, 2004, **108**, 3410–3425.
31 C. W. Carpenter, C. Dhong, N. B. Root, D. Rodriquez, E. E. Abdo, K. Skelil, M. A. Alkhadra, J. Ramírez, V. S. Ramachandran and D. J. Lipomi, *Mater. Horiz.*, 2018, **5**, 70–77.
32 J. D. Glover, C. E. McLaughlin, M. K. McFarland and J. T. Pham, *J. Polym. Sci.*, 2020, **58**, 343–351.
33 L. Skedung, M. Arvidsson, J. Y. Chung, C. M. Stafford, B. Berglund and M. W. Rutland, *Sci. Rep.*, 2013, **3**, 2617.
34 E. AliAbbasi, V. Aydingul, A. Sezgin, U. Er, S. Turkuz and C. Basdogan, *IEEE Trans. Haptics*, 2023, **16**, 586–593.
35 S. R. Wasserman, Y. T. Tao and G. M. Whitesides, *Langmuir*, 1989, **5**, 1074–1087.
36 M. Zhu, M. Z. Lerum and W. Chen, *Langmuir*, 2012, **28**, 416–423.
37 S. Das, N. Cadirov, S. Chary, Y. Kaufman, J. Hogan, K. L. Turner and J. N. Israelachvili, *J. R. Soc. Interface*, 2015, **12**, 20141346.
38 G. A. D. Briggs and B. J. Briscoe, *Philos. Mag. A*, 1978, **38**, 387–399.
39 T. Baumberger, C. Caroli and O. Ronsin, *Phys. Rev. Lett.*, 2002, **88**, 075509.
40 C. J. Rand and A. J. Crosby, *J. Appl. Phys.*, 2009, **106**, 064913.
41 K. Viswanathan, N. K. Sundaram and S. Chandrasekar, *Soft Matter*, 2016, **12**, 9185–9201.
42 B. N. J. Persson, O. Albohr, C. Creton and V. Peveri, *J. Chem. Phys.*, 2004, **120**, 8779–8793.
43 D. Maksuta, S. Dalvi, A. Gujrati, L. Pastewka, T. D. B. Jacobs and A. Dhinojwala, *Soft Matter*, 2022, **18**, 5843–5849.
44 F. A. A. Kingdom and N. Prins, *Psychophysics: A Practical Introduction*, Academic Press, 2016.
45 X.-D. Xiao, G. Liu, D. H. Charych and M. Salmeron, *Langmuir*, 1995, **11**, 1600–1604.
46 R. Sahli, A. Prot, A. Wang, M. H. Müser, M. Piovarči, P. Didyk and R. Bennewitz, *Sci. Rep.*, 2020, **10**, 15800.
47 Y. L. Chen, C. A. Helm and J. N. Israelachvili, *J. Phys. Chem.*, 1991, **95**, 10736–10747.
48 A. Lio, D. H. Charych and M. Salmeron, *J. Phys. Chem. B*, 1997, **101**, 3800–3805.
49 X. Xiao, J. Hu, D. H. Charych and M. Salmeron, *Langmuir*, 1996, **12**, 235–237.
50 C. Drummond and J. Israelachvili, *Phys. Rev. E*, 2001, **63**, 041506.

51 B. C. Donose, E. Taran, I. U. Vakarelski, H. Shinto and K. Higashitani, *J. Colloid Interface Sci.*, 2006, **299**, 233–237.
52 T. Yoshioka, J. C. Craig, G. C. Beck and S. S. Hsiao, *J. Neurosci.*, 2011, **31**, 17603–17611.
53 M. Fehlberg, E. Monfort, S. Saikumar, K. Drewing and R. Bennewitz, *IEEE Trans. Haptics*, 2024, **17**, 957–963.
54 M. J. Adams, S. A. Johnson, P. Lefèvre, V. Lévesque, V. Hayward, T. André and J.-L. Thonnard, *J. R. Soc. Interface*, 2013, **10**, 20120467.
55 I. Waters, A. Alazmani and P. Culmer, *IEEE Trans. Med. Robot. Bionics*, 2020, **2**, 541–544.